Proceedings of the International Association for Shell and Spatial Structures (IASS) Symposium 2010, Shanghai
Spatial Structures – Permanent and Temporary
November 8-12 2010, Shanghai, China

A Structural System for the Retractable Loop-Dome

Tsutomu Kokawa

Dr. Eng., Professor, School of Design, Tokai University
Kamuicho Chuwa 224, Asahikawa, Japan
kokawa@tspirit.tokai-u.jp

Abstract

This paper proposes a new structural system for the Retractable Loop-Dome (RLD) that comprises a main structure and a substructure. The main structure consists of 3-dimensional multi-angulated scissor elements (3-DMASEs) in lamella arrangement. The substructure comprises a part of an Aspension Dome, an outer tension cable disposed concentrically around the peripheral border and zigzag cables in a ring of quadrilaterals of the lamella. The Aspension Dome part, the central part of the RLD, comprises hoop cables, diagonal cables and posts. 3-DMASEs, posts and diagonal cables are fixed members. All members are always under stress while keeping the equilibrium of the RLD by simultaneously adjusting the length and the tension forces of the hoop cables, the outer tension cable and the zigzag cables. The tension forces of these cables are determined numerically by solving a nonlinear programming problem subjected to constraints.

Keywords: retractable loop-dome, 3-dimensional multi-angulated scissor element, main structure, substructure, structural system, nonlinear programming

1 Introduction

In the preceding papers [1][2], the author proposed the retractable loop-dome (RLD) that continuously changes in shape according to variations in the diameter of the oculus. The main structural elements of the RLD are 3-dimensional multi-angulated scissor elements (3-DMASEs) in lamella arrangement. The geometric form of the scissor element is determined by cutting a sphere with an inclined plane that intersects the apex. The pivots of the scissor elements form a perfect circle at each level, and are arranged at an equiangular degree around the axis of the dome. The scissor pivot-axes coincide with the normals of the spherical surface. The main structure of the RLD consists of two sets of 3-DMASEs, one set running clockwise and the other counterclockwise from the center. This allows the changes in the geometry of the structure, particularly the diameter of the oculus, without elastic deformation of the elements. During the retraction, a small variation in angle is caused by a slight difference between the scissor pivot-axis and the hole-axis, necessitating a loose-hole or an embedded spherical roller bearing (or self-aligning ball bearings) at the scissor pivot. In order to apply the main structure for practical use, the structure must be made stable. Therefore, a structural system in which an expandable ring is added to both the inner and outer circle of the main structure, so as to produce the structural efficiency of shell-like behavior, was proposed [1][2]. However, in the proposal, there was a problem in making the inner ring actual because of a large expansion-traction ratio and action in high compression despite using telescopic cylinder rods.

This paper briefly describes the three ideas considered thus far in the development of a structural system for the RLD. Comparing them from the aspect of constructional and structural rationality, one appears to have the most potential for allowing the realization of the RLD. This newest structural system comprises the main structure and a substructure. The substructure comprises a part of an Aspension Dome [3], an outer tension cable disposed concentrically around the peripheral border of the main structure and zigzag cables in a ring of quadrilaterals of the lamella. The Aspension Dome part, the central part of the RLD, comprises hoop cables, diagonal cables and posts.

The 3-DMASEs, posts and diagonal cables are fixed members. Those members are always under stress while keeping the equilibrium of the RLD by simultaneously adjusting the length and the tension forces of the hoop cables, the outer tension cable and the zigzag cables. Based on the structural analysis developed in this paper, the tension forces of those cables are determined numerically by solving a nonlinear programming problem subjected to constraints. Some numerical examples are shown.

2 Main structure

The main structure of the RLD consists of 3-DMASEs in lamella arrangement. The geometric form of the 3-DMASE is determined by cutting a sphere with a plane. The scissor hinge-points (1, 2, …, *i*, *i*+1, ..., *n*) of the element are arranged on the surface of a sphere S as follows:

a) Cutting sphere S with inclined plane P that intersects apex T, as shown in Fig. 1(a).

b) Arranging hinge-points on circle Q (ellipse on the *xy* plane), as shown in Fig. 1(b). That is, $\theta_2-\theta_1=\theta_3-\theta_2=\ldots=\theta_{(i+1)}-\theta_i=\ldots=\theta_n-\theta_{(n-1)}=\Delta\theta$ on *xy* plane. Referring to Fig.1 and denoting a changing form parameter *t* explained in the previous paper [1], 3-dimensional coordinate of a scissor point *i* which is written 'node (point) *i*' in the following, is given by Eq.(1).

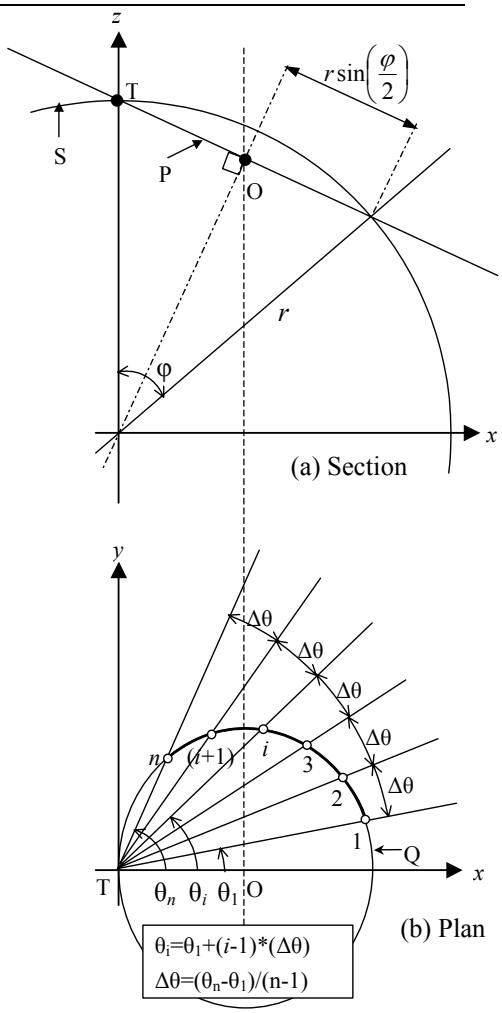

Fig.1 Position of scissor points

When *t*=0, it is called 'the reference state', the scissor pivot-axes coincide with the normals of the spherical surface. The main structure of the RLD consists of two sets of 3-DMASEs, one set running clockwise and the other counterclockwise from the center. This allows the changes in the geometry of the structure, particularly the diameter of the oculus as shown in Fig.2, without elastic deformation of the elements.

$$\frac{x_i}{r}=X_i=\frac{\sin\varphi\left\{\cos t+\cos\left(\frac{\varphi}{2}\right)\sin t\tan\theta_i\right\}}{1+\cos^2\left(\frac{\varphi}{2}\right)\tan^2\theta_i},\quad \frac{y_i}{r}=Y_i=\tan\theta_i X_i,\quad \frac{z_i}{r}=Z_i=1-\tan\left(\frac{\varphi}{2}\right)X_i \tag{1}$$

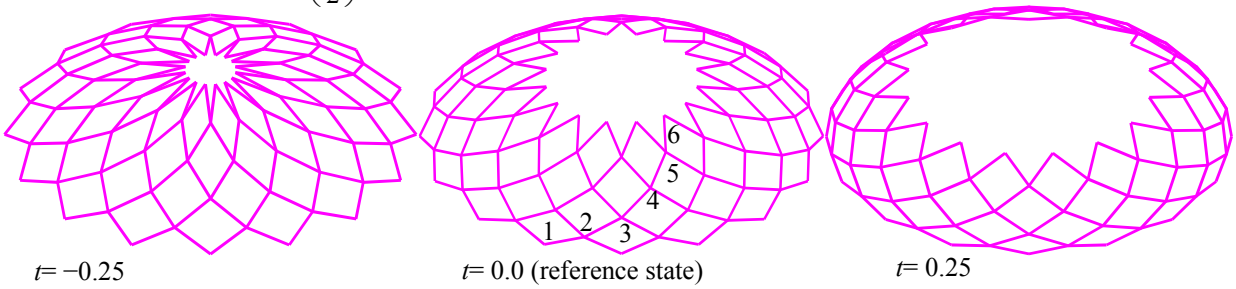

t= −0.25 *t*= 0.0 (reference state) *t*= 0.25

Fig.2 Changing geometry of main structure (*n*=6)

3 Proposed structural systems

In order to apply the main structure for practical use, the structure must be made stable. The problem lies in establishing a rational structural system for a large span, considering the expansion-traction technology of today. The two ideas previously put forth concerning the structural system of the RLD, along with the new idea, are described as follows.

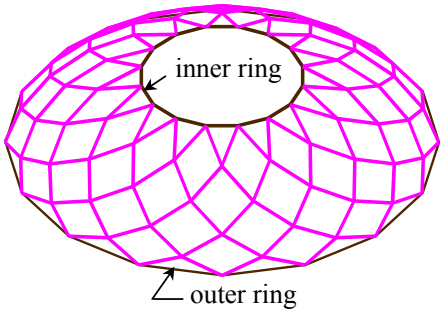

Fig.3 System A

3.1 System A (main structure + (inner+outer) expandable ring)

As shown in Fig. 3, system A, an expandable ring is added to both the inner and outer circles of the dome so as to produce the structural efficiency of shell-like behavior under dead load. Each expandable circular ring consists of expandable rods that form a regular polygon. In the case of the outer ring receiving tension, such a rod may in practice be possible to make by using electrical or hydraulic control technology because of its small expansion-traction ratio. On the other hand, in the case of the inner ring, which is indispensable to the rational structural system of the RLD, there is an actualization problem because of the large expansion-traction ratio 5~6 and action in high compression (Fig. 4).

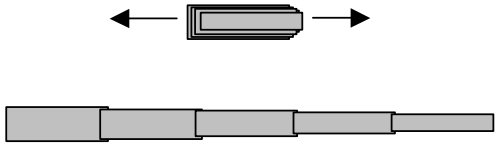

Fig.4 Telescopic cylinder

3.2 System B (main structure + (secondary inner ring + suspension+ outer ring)

The inner ring through node 5 in Fig.5, shifted from the position laid down in the innermost inner ring of System A, is called the secondary inner ring, and has a maximum expansion-traction ratio within 3. This system provides solutions to the problems in System A. However, in this system, a big bending moment occurs at node 5 and its vicinity in the cantilever section between nodes 5 and 6. A tension cable connected at the top of the post on node 5, suspends node 6. The secondary inner ring, outer ring and either suspension cable or stay cable have to control the length of the members during the change in shape of the RLD. This difficulty arises from the telescopic cylinder's tendency to buckle. The production of the secondary inner ring is still difficult because of the action in high compression although the expansion-traction ratio is smaller than that of system A.

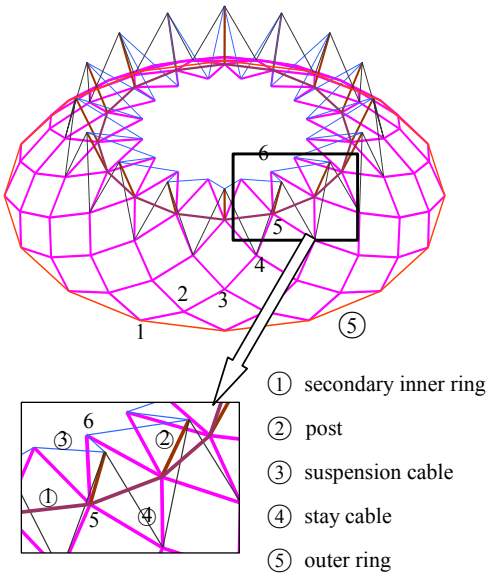

Fig.5 System B

3.3 New system (main structure +(a part of Aspension dome' system + zigzag cable + outer ring))

The expandable compression member drives the RLD in both systems A and B. This member works under high compression and must change length at the same time. In this situation, a telescopic cylinder may be adopted as the expandable member. However a telescopic cylinder normally lacks bending rigidity where the rods are connected. Therefore, there is a buckling problem that affects the structural stability. This considered, the expandable compression member may not be practicable for driving the RLD. In contrast, the new system employs adjustment of length and tension of the cables

to change the geometry of the RLD. The new structural system of the RLD comprises the main structure and a substructure, as shown in Fig. 6. The substructure comprises a part of an Aspension Dome [3], an outer tension cable disposed concentrically around the peripheral border of the main structure and zigzag cables connected in a W-M shaped pattern to the points of the concentric ring of quadrilaterals of the lamella. The Aspension Dome part, the central part of the RLD, comprises hoop cables, diagonal cables and posts. 3-DMASEs, posts and diagonal cables are fixed members. These members are always under stress while keeping the equilibrium of the RLD by simultaneously adjusting the length and the tension forces of the hoop cables, outer tension cable and zigzag cables. Fig. 7 shows a diagram of this structural system. Referring to the figure, appropriate horizontal forces are given to nodes 6, 7 and 8 by adjusting the length and the tension forces of the hoop cables ⑤. While, diagonal cables ③ act in tension and posts ② act in compression. The posts are raised and the power opposite to the direction of gravity acts on the nodes of the main structure. The tension force of the diagonal cable ③ acts on node 4 and shrinking action occurs in the circumferential direction of the RLD. The zigzag cable ④, together with the main structure, effectively resists against the shrinking action. The outer cable ⑥ is indispensable for containing the spreading action of the RLD. The hoop cables through node 6 and 8 resist the lifting force of the wind load. This new system creates a self-equilibrium structure. The tension forces of these cables are determined numerically by solving a nonlinear programming problem subjected to constraints.

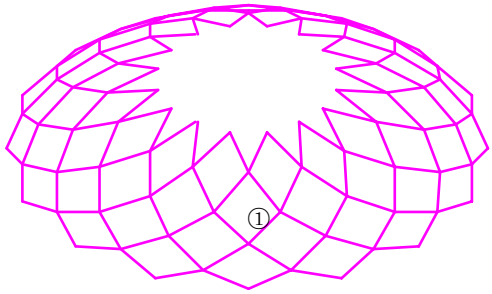

(3-DMASEs ① in lamella arrangement)

Fig. 6(a) Main structure

+

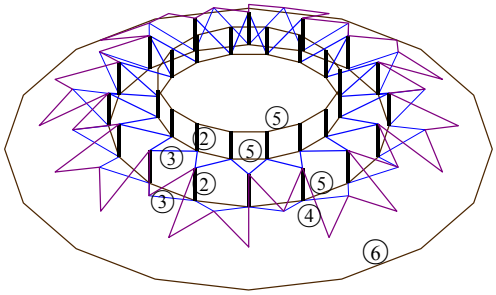

②post ③diagonal cable ④zigzag cable ⑤hoop cable
⑥outer cable (: member's changing in length)

Fig. 6(b) Substructure

| |

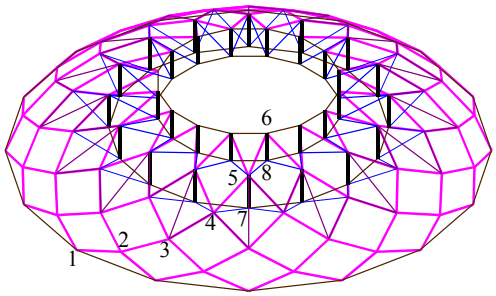

Fig. 6 New structural system

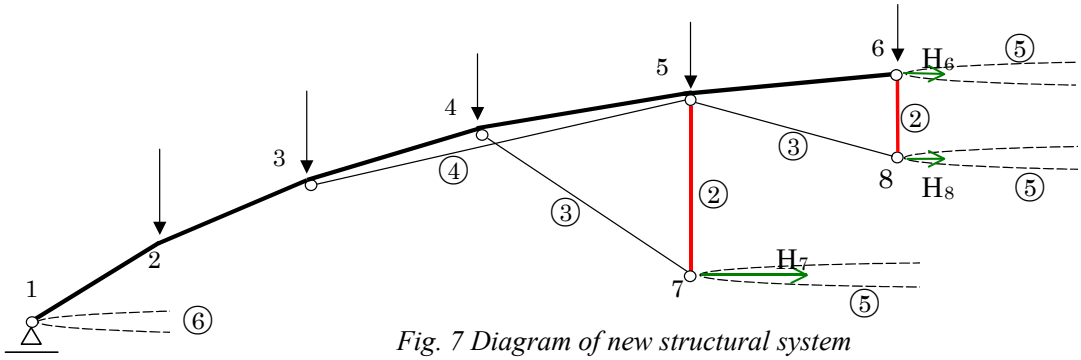

Fig. 7 Diagram of new structural system

4 Numerical method of structural analysis

According to the comparison from the stand point of constructional and structural rationality, the new structural system appears to have the most potential for allowing the realization of the RLD. A numeric method of structural analysis is described in order to investigate the structural behaviors in each RLD system under an axisymmetric dead load, and the comparison among the three systems is made numerically. The results show the new structural system to have significantly better structural performance than systems A and B. Furthermore, structural analysis of the RLD based on the new system is carried out in a wide range of *t*.

4.1 Stiffness matrix of 3-DMASE

Fig. 8 shows the space position of major points expressed in (*x*, *y*, *z*) 3-dimensional coordinates for a beam-column element i connecting scissor points between *i* and (*i*+1) of 3-DMASE. In the figure, 3-dimensional coordinates of node *i* are already given in Eq.(1). In addition to these coordinates, the coordinates of node (*i*+1), the central point C_i of the beam-column element i and the sphere centre point *P* are given in Eq. (2).

$$\begin{Bmatrix} x_{(i+1)} \\ y_{(i+1)} \\ z_{(i+1)} \end{Bmatrix} = \begin{Bmatrix} r\dfrac{\sin\varphi\left\{\cos t + \cos\left(\dfrac{\varphi}{2}\right)\sin t \tan\theta_{(i+1)}\right\}}{1+\cos^2\left(\dfrac{\varphi}{2}\right)\tan^2\theta_{(i+1)}} \\ \tan\theta_{(i+1)}x_{(i+1)} \\ r-\tan\left(\dfrac{\varphi}{2}\right)x_{(i+1)} \end{Bmatrix}, \quad \begin{Bmatrix} c_{xi} \\ c_{yi} \\ c_{zi} \end{Bmatrix} = \begin{Bmatrix} \dfrac{x_i + x_{(i+1)}}{2} \\ \dfrac{y_i + y_{(i+1)}}{2} \\ \dfrac{z_i + z_{(i+1)}}{2} \end{Bmatrix}, \quad \begin{Bmatrix} p_x \\ p_y \\ p_z \end{Bmatrix} = r\begin{Bmatrix} \dfrac{\sin\varphi(\cos t - 1)}{2} \\ \sin\left(\dfrac{\varphi}{2}\right)\sin t \\ \sin^2\left(\dfrac{\varphi}{2}\right)(1-\cos t) \end{Bmatrix} \quad (2)$$

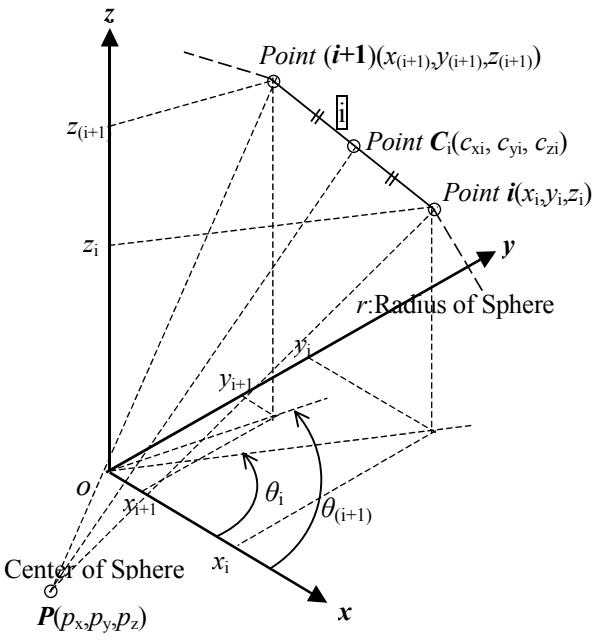

Fig. 8 3-dimensional coordinates of points

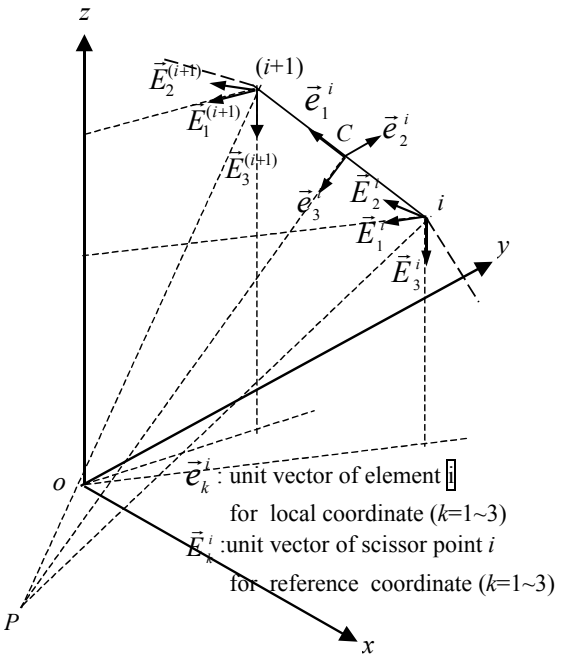

Fig. 9 Base unit orthogonal vectors

Fig. 9 shows three sets of orthogonal components of unit vector $\vec{e}_k^{\,i}$ (k=1, 2, 3) for the local coordinate and three sets of orthogonal components of unit vector $\vec{E}_k^{\,i}$ (k=1, 2, 3) for the reference coordinate. Those unit vectors are given in Eq. (3).

$$
\begin{aligned}
&\vec{e}_1^{\,i} = \frac{1}{l_i}\left(x_{(i+1)} - x_i, y_{(i+1)} - y_i, z_{(i+1)} - z_i\right) && \vec{E}_1^{\,i} = \left(-\frac{x_i}{R_i}, -\frac{y_i}{R_i}, 0\right) && \vec{E}_1^{(i+1)} = \left(-\frac{x_{(i+1)}}{R_{(i+1)}}, -\frac{y_{(i+1)}}{R_{(i+1)}}, 0\right)\\
&\vec{e}_3^{\,i} = \frac{1}{s_i}\left(p_x - c_{xi}, p_y - c_{yi}, p_z - c_{zi}\right) && R_i = \sqrt{x_i^{\,2} + y_i^{\,2}} && R_{(i+1)} = \sqrt{x_{(i+1)}^{\,2} + y_{(i+1)}^{\,2}}\\
&\vec{e}_2^{\,i} = \vec{e}_3^{\,i} \times \vec{e}_1^{\,i} && \vec{E}_2^{\,i} = \left(-\frac{y_i}{R_i}, \frac{x_i}{R_i}, 0\right) && \vec{E}_2^{(i+1)} = \left(-\frac{y_{(i+1)}}{R_{(i+1)}}, \frac{x_{(i+1)}}{R_{(i+1)}}, 0\right)\\
&l_i = \sqrt{\left(x_{(i+1)} - x_i\right)^2 + \left(y_{(i+1)} - y_i\right)^2 + \left(z_{(i+1)} - z_i\right)^2} && \vec{E}_3^{\,i} = (0,0,-1) && \vec{E}_3^{(i+1)} = (0,0,-1)\\
&s_i = \sqrt{\left(p_x - c_{xi}\right)^2 + \left(p_y - c_{yi}\right)^2 + \left(p_z - c_{zi}\right)^2}
\end{aligned}
\qquad (3)
$$

The components of end force with respect to both the local and reference system of axes are defined in Fig. 10 for the beam-column element i. And the components of end displacement with respect to both systems are defined as well, although not shown in the figure.

The stiffness equation for the element i with respect to the local system is given by Eq.(4).

$$\{f\}_i = [k]_i \{d\}_i \qquad (4)$$

Where $\{f\}_i$ is 12 sets of end force vector referred in Fig.10(a), and $\{d\}_i$ is the corresponding 12 sets of nodal displacement vector. The transpose of the vectors, $\{f\}_i$ and $\{d\}_i$, are written in Eq.(5).

$$
\begin{aligned}
\{f\}_i^{\,t} &= \left(n_{i1} \quad n_{i2} \quad n_{i3} \quad m_{i1} \quad m_{i2} \quad m_{i3} \quad n_{(i+1)1} \quad n_{(i+1)2} \quad n_{(i+1)3} \quad m_{(i+1)1} \quad m_{(i+1)2} \quad m_{(i+1)3}\right)\\
\{d\}_i^{\,t} &= \left(\delta_{i1} \quad \delta_{i2} \quad \delta_{i3} \quad \theta_{i1} \quad \theta_{i2} \quad \theta_{i3} \quad \delta_{(i+1)1} \quad \delta_{(i+1)2} \quad \delta_{(i+1)3} \quad \theta_{(i+1)1} \quad \theta_{(i+1)2} \quad \theta_{(i+1)3}\right)
\end{aligned}
\qquad (5)
$$

Where δ_{ik}(k=1~3)=translation, θ_{ik}(k=1~3)=rotation with respect to the local coordinate axes. $[k]_i$ is the 12×12 size of beam-column type of member stiffness matrix and given by Eq.(6).

$$
[k]_i = \begin{bmatrix}
\frac{EA_i}{l_i} & 0 & 0 & 0 & 0 & 0 & -\frac{EA_i}{l_i} & 0 & 0 & 0 & 0 & 0\\
 & \frac{12EI_{i3}}{l_i^3} & 0 & 0 & 0 & \frac{6EI_{i3}}{l_i^2} & 0 & -\frac{12EI_{i3}}{l_i^3} & 0 & 0 & 0 & \frac{6EI_{i3}}{l_i^2}\\
 & & \frac{12EI_{i2}}{l_i^3} & 0 & -\frac{6EI_{i2}}{l_i^2} & 0 & 0 & 0 & -\frac{12EI_{i2}}{l_i^3} & 0 & -\frac{6EI_{i2}}{l_i^2} & 0\\
 & & & \frac{GI_{i1}}{l_i} & 0 & 0 & 0 & 0 & 0 & -\frac{GI_{i1}}{l_i} & 0 & 0\\
 & & & & \frac{4EI_{i2}}{l_i} & 0 & 0 & 0 & \frac{6EI_{i2}}{l_i^2} & 0 & \frac{2EI_{i2}}{l_i} & 0\\
 & & & & & \frac{4EI_{i3}}{l_i} & 0 & -\frac{6EI_{i3}}{l_i^2} & 0 & 0 & 0 & \frac{2EI_{i3}}{l_i}\\
 & & & & & & \frac{EA_i}{l_i} & 0 & 0 & 0 & 0 & 0\\
 & & & & & & & \frac{12EI_{i3}}{l_i^3} & 0 & 0 & 0 & -\frac{6EI_{i3}}{l_i^2}\\
 & & & & & & & & \frac{12EI_{i2}}{l_i^3} & 0 & \frac{6EI_{i2}}{l_i^2} & 0\\
 & & & & & & & & & \frac{GI_{i1}}{l_i} & 0 & 0\\
 & & & & & & & & & & \frac{4EI_{i2}}{l_i} & 0\\
 & & & & & & & & & & & \frac{4EI_{i3}}{l_i}
\end{bmatrix}
\qquad (6)
$$

SYM.

Where E=Young's modulus, A_i=cross-sectional area, l_i=element length, I_{i1}=torsional constant, $I_{i(2,3)}$ =moment of inertia and G=shearing modulus for the element i.

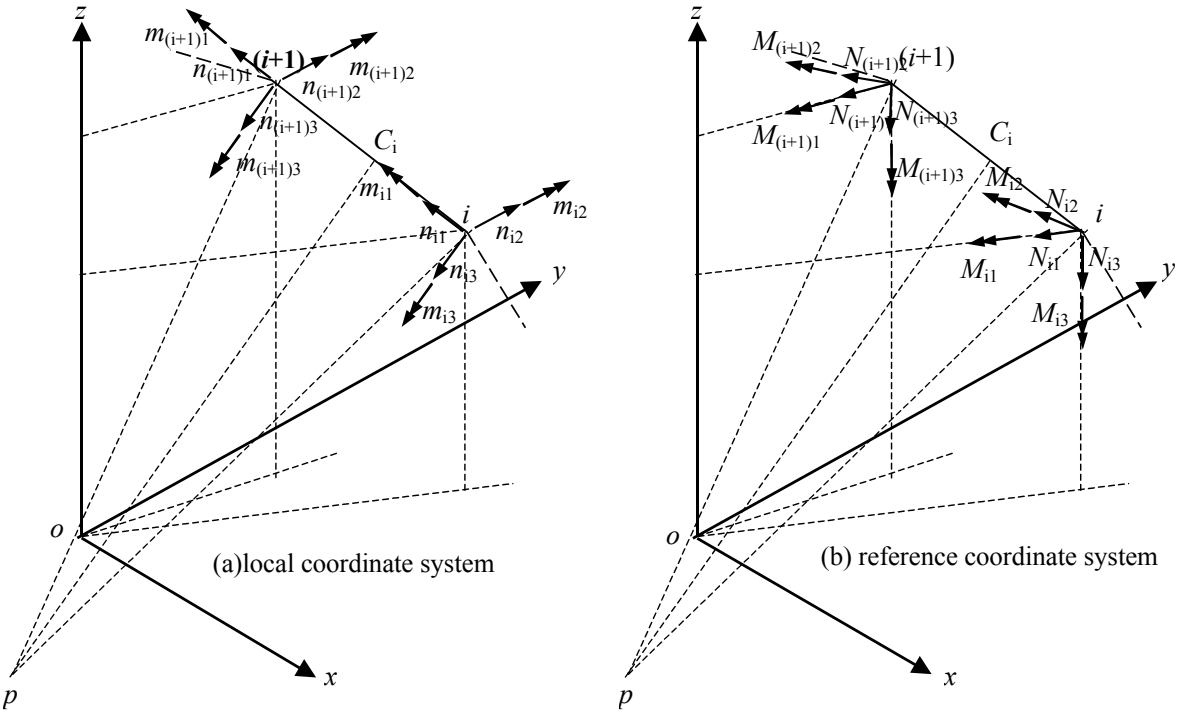

Fig. 10 Components of end force for element i

The stiffness equation for the element i with respect to the reference coordinate system is given by Eq. (7).

$$\{F\}_i = [K]_i \{D\}_i \qquad (7)$$

Where $\{F\}_i$ is 12 sets of end force vector referred to Fig.10(b), and $\{D\}_i$ is the corresponding 12 sets of nodal displacement vector. The transpose of the vectors, $\{F\}_i$ and $\{D\}_i$, are written in Eq.(8).

$$\{F\}_i^t = \{N_{i1} \quad N_{i2} \quad N_{i3} \quad M_{i1} \quad M_{i2} \quad M_{i3} \quad N_{(i+1)1} \quad N_{(i+1)2} \quad N_{(i+1)3} \quad M_{(i+1)1} \quad M_{(i+1)2} \quad M_{(i+1)3}\} \qquad (8)$$

$$\{D\}_i^t = \{\Delta_{i1} \quad \Delta_{i2} \quad \Delta_{i3} \quad \Theta_{i1} \quad \Theta_{i2} \quad \Theta_{i3} \quad \Delta_{(i+1)1} \quad \Delta_{(i+1)2} \quad \Delta_{(i+1)3} \quad \Theta_{(i+1)1} \quad \Theta_{(i+1)2} \quad \Theta_{(i+1)3}\}$$

The components of end displacement and the corresponding components of end force with respect to both the local and reference systems are given by Eq. (9).

$$\{d\}_i = [T]_i \{D\}_i, \quad \{f\}_i = [T]_i \{F\}_i \qquad (9)$$

Where $[T]_i$ is defined as the transformation matrix for the element i and written in Eq. (10).

$$[T]_i = \begin{bmatrix} [T_1]_i & [0] & [0] & [0] \\ [0] & [T_1]_i & [0] & [0] \\ [0] & [0] & [T_2]_i & [0] \\ [0] & [0] & [0] & [T_2]_i \end{bmatrix}, \quad [T_1]_i = \begin{bmatrix} \vec{e}_1^{\,i} \cdot \vec{E}_1^{\,i} & \vec{e}_1^{\,i} \cdot \vec{E}_2^{\,i} & \vec{e}_1^{\,i} \cdot \vec{E}_3^{\,i} \\ \vec{e}_2^{\,i} \cdot \vec{E}_1^{\,i} & \vec{e}_2^{\,i} \cdot \vec{E}_2^{\,i} & \vec{e}_2^{\,i} \cdot \vec{E}_3^{\,i} \\ \vec{e}_3^{\,i} \cdot \vec{E}_1^{\,i} & \vec{e}_3^{\,i} \cdot \vec{E}_2^{\,i} & \vec{e}_3^{\,i} \cdot \vec{E}_3^{\,i} \end{bmatrix}, \quad [T_2]_i = \begin{bmatrix} \vec{e}_1^{\,i} \cdot \vec{E}_1^{\,(i+1)} & \vec{e}_1^{\,i} \cdot \vec{E}_2^{\,(i+1)} & \vec{e}_1^{\,i} \cdot \vec{E}_3^{\,(i+1)} \\ \vec{e}_2^{\,i} \cdot \vec{E}_1^{\,(i+1)} & \vec{e}_2^{\,i} \cdot \vec{E}_2^{\,(i+1)} & \vec{e}_2^{\,i} \cdot \vec{E}_3^{\,(i+1)} \\ \vec{e}_3^{\,i} \cdot \vec{E}_1^{\,(i+1)} & \vec{e}_3^{\,i} \cdot \vec{E}_2^{\,(i+1)} & \vec{e}_3^{\,i} \cdot \vec{E}_3^{\,(i+1)} \end{bmatrix} \qquad (10)$$

Using Eq. (5), (7), (9) and (10), the stiffness matrix $[K]_i$ for the element i with respect to the reference coordinate system is given by Eq. (11).

$$[K]_i = [T]_i^t [k]_i [T]_i \qquad (11)$$

Then, by superimposing Eq. (11), the overall stiffness equation of 3-DMASE with respect to the reference coordinate system is obtained.

4.2 Overall stiffness equation

The overall stiffness equation for the RLD for each structural system under axisymetric loading conditions can be obtained by superimposing the stiffness equations with respect to the reference coordinate for the additional members in each structural system on the above-mentioned stiffness equation for 3-DMASE. In this case, the overall equation is solved under the boundary displacement conditions that Δ_3=0 for node point 1 and Δ_2=0 for all node points.
In the new structural system for the RLD, a set of horizontal loads act on the reference direction 1 through the stressing of hoop cables, in addition to the dead load applied in the reference direction 3. Referring to Fig. 7, three sets of horizontal loads H_6, H_7 and H_8 are determined by solving the following nonlinear problem subjected to constraints in the numerical structural analysis.
The nonlinear programming problem: Minimize the sum of squares of nodal displacements in the main structure under the conditions that H_6, H_7 and H_8 work in tension. The numerical calculation is based on Powell's variable metric method [4].

4.3 Comparison between systems

The structural performances for the new structural system and the other two systems are investigated numerically based on the method of analysis in section 4.2. Fig. 11 shows the numerical comparison of nodal displacements, bending moments and axial force for t=0 using the following parameter.
Distribution of nodal vertical load: P_1=0, P_2=P_3= P*1.0, P_4= P*0.9, P_5= P*0.8, P_6= P*0.7 where P_i is the concentrated vertical load at node i and P is magnitude of load.
Data of 3-DMASE:
Geometry (see Fig.1): φ=45°, n=6, θ_1=15°, θ_6=71.25°, Δθ=11.25°, circumferential division number of dome=16
Member information: λ_1=200, λ_2=250, λ_3=200. Each λ is defined as r/i where i is the radii of gyration for each local axis and is calculated from $\sqrt{I/A}$. I is moment of inertia or torsional constant for each local axis and A is the sectional area. I and A are the same for all elements of 3-DMASE.
Additional member data:
System A: sectional area of the inner and the outer ring is taken to be the same as A of 3-DMASE.
System B: direction of post for t=0 is the normal of the spherical surface, length is 0.175*r, sectional area is 0.4*A, sectional area of suspension and stay cables is 0.2*A, length of post and stay cable is constant under retraction, sectional area of outer cable is A.
New system: direction of two posts for t=0 is vertical, sectional area of two posts = 0.4*A, length of inner post = 1.5*(z_6-z_8), length of secondary inner post = 3.0*(z_5-z_7), sectional area of diagonal cable = 0.2*A, sectional area of zigzag cable = 0.4*A, sectional area of outer cable = A, length of

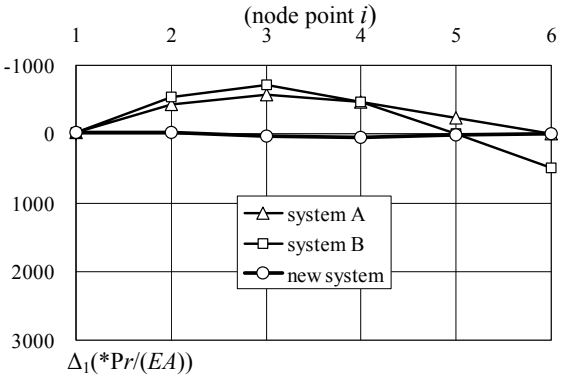

Fig. 11(a) Δ_1

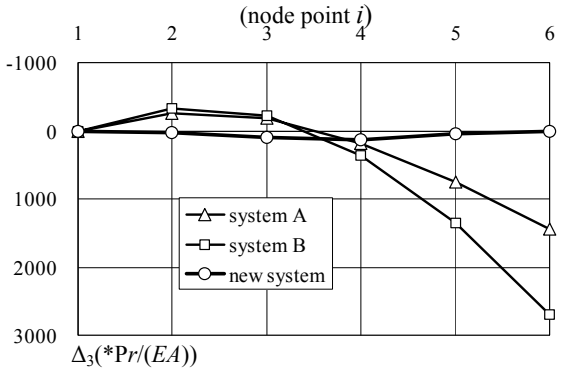

Fig. 11(b) Δ_3

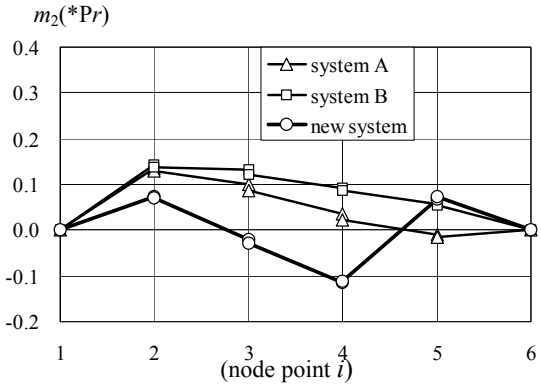

Fig. 11(c) m_2

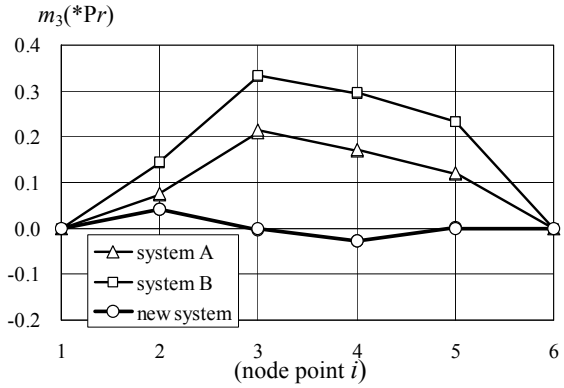

Fig. 11(d) m_3

posts and diagonal cables is constant under retraction.

In the analysis of the new system, H_6=0., H_7= 2.562*P and H_8=0. are the numerical solution for the given nonlinear programming problem. Referring to Fig. 11(a)(b)(d), the displacements and the bending moment with respect to the local axis 3 for the new structural system are very small compared to those of systems A and B. Referring to Fig.11(c)(d), a large bending moment with respect to the local axis 2 occurs at node 4, and the axial forces of elements 3 and 4 are relatively large, because the tension force of the zigzag cable acts on node 4 through H_7. Overall, the structural performance of the new structural system is significantly better than that of systems A and B.

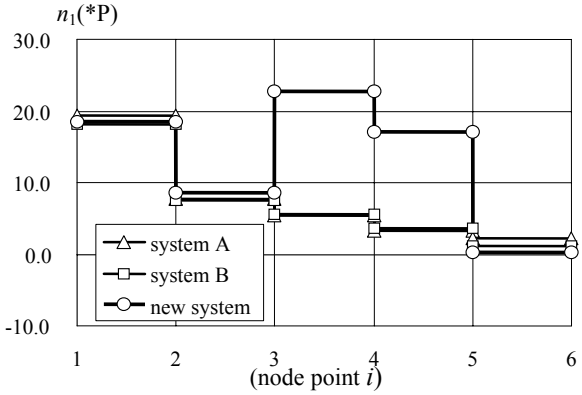

Fig. 11(e) n_1

4.4 Numerical results of new system

Concerning the new system, which indicates the best structural performance among the three proposed systems, its numerical structural analysis is carried out in a geometrical range where t= −0.25 ~ 0.25. The horizontal forces H_6, H_7 and H_8 are determined so as to minimize the sum of squares of nodal displacements in the main structure under the conditions that the hoop cables work in tension. Referring to Fig. 12, the nodal displacements and member forces change significantly in the range of t from –0.25 to 0.25. A large vertical displacement occurs at t= –0.25 and 0.25, and a large bending moment with respect to the local axis 2 occurs at node 4 where t=0.25. Fig.13 shows

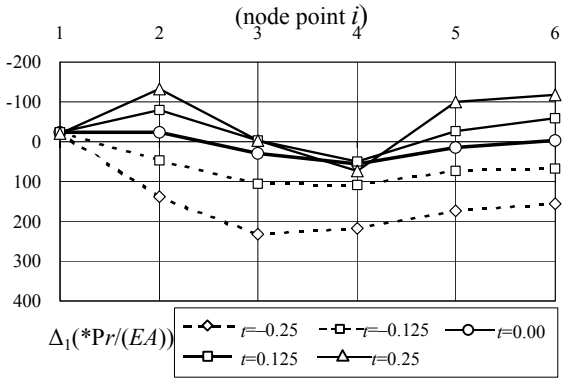

Fig. 12(a) Δ_1

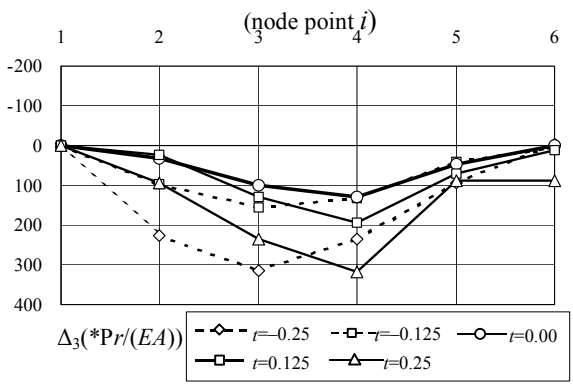

Fig. 12(b) Δ_3

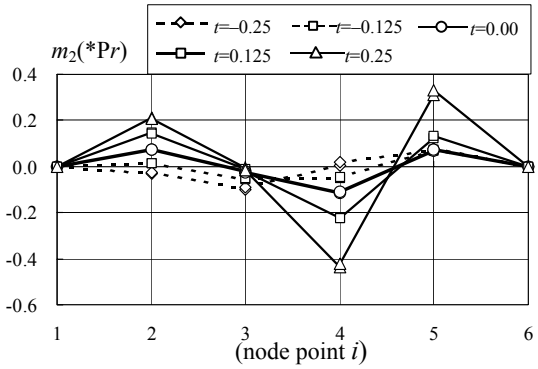

Fig. 12 (c) m_2

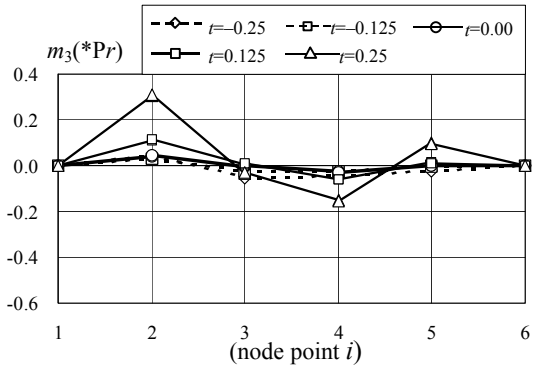

Fig. 12(d) m_3

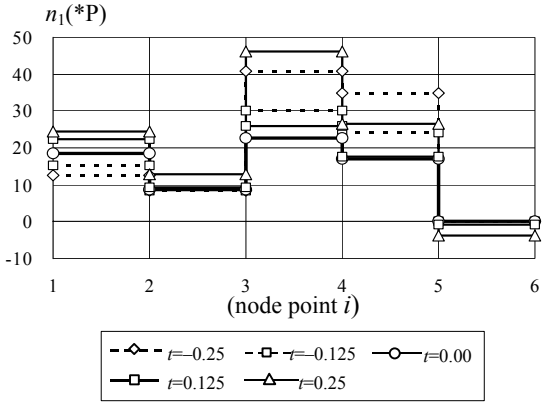

Fig. 12(e) n_1

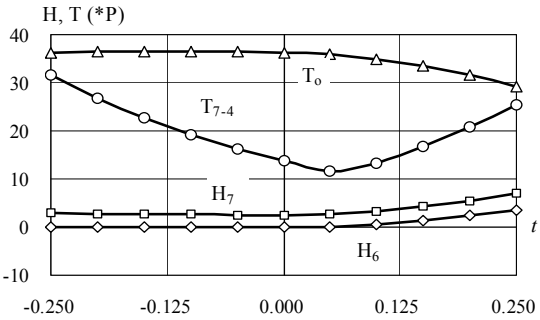

H_7,H_6:horizontal force (see Fig.7)
T_o,T_{7-4}: tension of outer ring, zigzag cable

Fig. 13 Horizontal forces, tension of cables

the variations in the horizontal forces H_6, H_7 and tension forces T_o, T_{7-4} for t. Although the other horizontal force H_8 is 0 for t in this analysis, the hoop cable through the node 8 may be useful in resisting a live load such as wind.

5 Ending remarks

For the RLD a new structural system that comprises a main structure and a substructure is proposed. The main structure consists of 3-DMASEs in lamella arrangement. The substructure comprises a part of an Aspension Dome, an outer tension cable disposed concentrically around the peripheral border of the main structure and zigzag cables in a concentric ring of quadrilaterals of the lamella. Based on structural analysis, the tension forces of these cables are determined numerically by solving a nonlinear programming problem subjected to constraints. According to the numerical results, new system maintains high level of structural performance throughout the changes in geometry. It seems that progress in the expansion-traction technology in high tension determines the realization of the RLD.

References

[1] Tsutomu Kokawa. Structural Idea of Retractable Loop-Dome. *JOURNAL OF THE IASS* Vol.41 (2000)n.2 August n.133, pp.111-116, 2000/08.

[2] Tsutomu Kokawa. Proposal of Retractable Loop-Dome. *CD-ROM of IASS in Nagoya* (Edited by Kunieda), TP148, 2001/10

[3] Richard Buckminster Fuller. ASPENSION (US3139957, Patented, July 7,1964). INVENTIONS THE PATENTED WORKS OF R. BUCKMINSTER FULLER, pp.201-213, ST. MARTIN'S PRESS. NEW YORK, 1983

[4] LPG1 Nonlinear programming (Powell's method using function values and its derivatives PP.482-486, SSL2.PDF), FUJITSU SSL II USER'S GUIDE(SCIENTIFIC SUBROUTINE LIBRARY), Fortran&C Academic Package V2.0L.10 B298C3921Z (CD-ROM)